# Absence of self-heated bistable resistivity in $La_{0.7}Sr_{0.3}MnO_3$ films up to high current densities

C. Moreno,* C. Munuera, A. Pérez del Pino, J. Gutiérrez, T. Puig, C. Ocal, and X. Obradors
*Institut de Ciéncia de Materials de Barcelona, CSIC, Campus UAB, 08193 Bellaterra, Catalonia, Spain*

A. Ruyter
*CNRS-CEA UMR 6157, LEMA–Université de Tours, Parc de Grandmont, 37000 Tours, France*
(Received 10 March 2009; revised manuscript received 26 June 2009; published 21 September 2009)

The $E(J)$ characteristics of well-characterized fully strained epitaxial $La_{0.7}Sr_{0.3}MnO_3$ films have been investigated up to high current densities ($J \sim 10^4 - 10^5$ A/cm$^2$). Different electric contact resistances and different current path configurations have been used to sort out the role of Joule self-heating from contact heating in the transport properties. It is demonstrated through macroscopic transport and conductive scanning force microscopy measurements that contact heating may lead to nonlinear and irreversible $E(J)$ characteristics when high contact resistances are used. Low dissipative contact power measurements are crucial to define the upper $J$ limits to keep linear and reversible $E(J)$ characteristics. We demonstrate that Joule self-heating in $La_{0.7}Sr_{0.3}MnO_3$ thin films only induces moderate warming at high temperatures while achieving bistable resistivity at low temperatures would require the use of very high current densities ($J \sim 5 \times 10^5$ A/cm$^2$).

DOI: 10.1103/PhysRevB.80.094412 PACS number(s): 73.40.Cg, 73.43.Jn, 73.63.Rt, 77.80.Fm

Resistive bistable switching can be used as a source of a generation more powerful and functional nonvolatile resistive random access memories (RRAM) and hence its development has generated a large interest.[1–8] Several types of oxides, such as $SrTiO_3$:Cr,[9] CuO,[10] NiO,[11] $TiO_2$,[6,12] and $Al_2O_3$,[13] have been shown to display electrically switchable resistive properties and multiple microscopic mechanisms have been proposed based either on redox processes involving cation or anion migration,[14] on the formation/rupture of conducting nanoscale filaments,[15–17] oxygen diffusion,[3] Mott metal-insulator transition,[4,18]variable Schottky barrier,[19] or charge trapping at interfacial sites.[20]

In manganites, the situation is even more complex and conflicting interpretations have been proposed. It has been suggested that bistable resistivity could be an intrinsic phenomenon associated to homogeneous Joule effect self-heating,[21] which would be therefore enhanced in measurements performed at high current densities ($J$) and which would depend on the sample dimensions and shape (bulk, thin film) because thermal heating and transfer would be deeply modified.

In order to elucidate the parameters controlling the resistance bistability, several manganite compositions have been investigated.[22–31] However, the influence of composition, intrinsic transport properties, and contact heating has not been clarified yet. Bistable resistivity in manganites of different compositions has been claimed to occur for polycrystalline ceramic, single crystal, and thin film materials where the self-heating effect and the electrical contacts influence might be very different. The intrinsic or extrinsic origin of the Joule heating effect remains therefore uncertain. In the case of the most robust ferromagnetic metal among the manganite series, $La_{0.7}Sr_{0.3}MnO_3$ (LSMO), which does not display any appreciable phase separation, bistable resistivity has been reported for thin films. However, it has not been clarified if it arises from Joule self-heating[24,25,32] or if it is an interface induced phenomenon.[33,34]

In this paper, we report on macroscopic transport measurements and local electrical behavior at the nanoscale, obtained by conducting scanning force microscopy (C-SFM) under low and high values of dissipative contact power ($DCP = \rho_c \times I^2 = R_c \times A_c \times I^2$), where $\rho_c$ is the contact resistivity, $R_c$ is the contact resistance, $A_c$ is the contact area, and $I$ is the current threading the sample. We will show that, while high DCP values induce hysteretic behavior, linear, and nonhysteretic $E(J)$ characteristics are obtained up to high $J$ values ($J \sim 5 \times 10^4$ A/cm$^2$) when low DCP are used. Moreover, beyond this limiting value only a moderate rise in temperature is induced without reaching a bistable resistivity regime. We suggest that to analyze Joule self-heating phenomena and if, eventually, intrinsic bistable resistivity exists, electrical contact heating should be minimized and a good thermal sample connection with a thermal bath must be used to avoid any unsuitable nuisance in the thermal transfer process.

$La_{0.7}Sr_{0.3}MnO_3$ films with a thickness of ~24 nm were grown by chemical solution deposition (CSD) on (100)$SrTiO_3$ (STO) substrates (5 mm × 5 mm × 0.5 mm). The metal-organic solution was deposited by spin coating, at 6000 rpm for 2 min, and annealed at temperatures in the range 900 °C–1000 °C under an oxygen gas flux, for different times, up to 12 h. Heteroepitaxial growth of LSMO films was confirmed by $\theta$-2$\theta$ x-ray diffraction (XRD) patterns and XRD $q$-plot measurements showed that the films are fully strained.[35,36]

Electrical transport measurements were performed in a PPMS Quantum Design system in a four-point configuration and magnetic measurements were carried out with a superconducting quantum interference device (SQUID) magnetometer provided with a 7 T magnet. To ensure well-defined geometries lithographed films were prepared through standard photolithography with track widths of 20 and 600 $\mu$m and voltage taps separated by 2 and 1.3 mm, respectively. To explore the influence of the contact resistance, different assemblies were used. Electrical contacts with high resistivity values ($\rho_c \sim 8.5$ $\Omega$ cm$^2$) consisted of wires directly attached to the film with Ag paste, whereas low resistivity contacts ($\rho_c < 0.2$ $\mu\Omega$ cm$^2$) were obtained by using Ag wires welded with indium to 1 $\mu$m-thick Ag contacts evaporated onto the

 

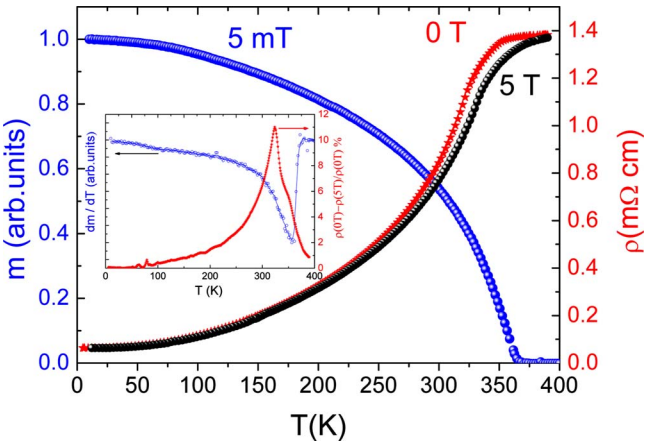


FIG. 1. (Color online) Main panel: temperature dependence of the resistivity under 0 and 5 T magnetic fields (right axis) and the magnetization in a magnetic field of 5 mT (left axis). Inset: temperature dependence of the magnetoresistance at 5 T and the magnetic moment derivative respect temperature dm/dT.

LSMO film. To avoid contact deterioration during the measurements, these Ag contacts were capped with 30 nm of Au and cured by annealing during one hour at 400 °C. To analyze the power dissipated at the structures, $E(J)$ measurements were carried out with different maximum currents. Thus, at room temperature experiments, we employed values up to 120 mA ($J \sim 10^5$ A/cm$^2$) for nonlithographed films and up to 5 and 0.1 mA for the 600 and 20 $\mu$m track width lithographed films, ($J=3\times10^4$ A/cm$^2$ and $J=2\times10^4$ A/cm$^2$, respectively).

C-SFM measurements were performed under low humidity conditions (2% RH in a $N_2$ flux) using a commercial head and software from Nanotec.[37] We used commercial conductive boron-doped diamond coated tips and cantilever force constants of $k=2.8$ N/m (Nanosensors). The conducting tip was biased and placed in contact with the sample, under controlled load, i.e., by using a normal force feedback, to measure the current flow as a function of the applied voltage. The same tip has been used in all the C-SFM experiments presented here to permit their direct comparison. As will be shown, dramatically different dissipative power conditions were obtained by performing $I$-$V$ curves either in direct tip-film contact or placing the tip on top of Au nanodots[38] previously dispersed by spin coating onto the LSMO film. A thermal treatment at 300 °C during 1 h was used after Au deposition to minimize the contact resistance.

We note that to make easier the paper's reading, throughout our paper, the experimental data will appear as they are commonly represented, i.e., $E(J)$ characteristics are shown for macroscopic measurements whereas current versus voltage ($I$-$V$) curves are used to illustrate the local measurements. The contact resistance in the later is then defined as the inverse slope of the linear region of the $I$-$V$ curves.

The quality of the grown LSMO films can be derived from data in Fig. 1, where the zero and 5 T field resistivity, as well as the magnetic moment at 5 mT after a field cooling process, are shown. The figure inset displays the corresponding magnetoresistance and the magnetization derivative, dm/dT, with the typical peak at $T_c$. The values of resistivity, magnetoresistance, and $T_c$ are very similar to those observed in LSMO films grown by physical vapor deposition techniques, such as sputtering or pulsed laser deposition, leading us to conclude that a similar epitaxial quality is achieved with films grown by our CSD approach.

Joule self-heating as a source of resistance bistability is a phenomenon which has been extensively investigated in normal metals and superconductors[21] and has been shown to result from a unique balance between heat release and heat transfer to the thermal bath. Provided the unit volume heat generation is determined by $Q(T)=\rho(T)J^2$, a bistable resistance of thermal origin can occur only if two particular $J$ values exist for which the corresponding $Q(T)$ values can be properly transferred to the thermal bath (via the anchored substrate) and hence a new isothermal steady state can be reached. Therefore, to achieve bistable resistance of thermal origin one should perform electrical transport measurements at enhanced Joule self-heating conditions, i.e., at $J$ values as high as possible. This poses the problem of electrical contact optimization which needs to be properly addressed and which deeply differs for thin film and bulk sample measurements. To analyze the importance of the contacts, we have carried out macroscopic transport measurements in LSMO thin films under different current configurations and electrical contact qualities, i.e., contacts with different DCP values.

Figure 2(a) presents a typical voltage-current characteristics curve measured in a standard nonlithographed film with a DCP of 17 W cm$^2$, a common situation on macroscopic transport studies of manganites. The curves are hysteretic and strongly temperature-dependent (not shown). This result reminds the well-known behavior observed in critical current measurements of high current density superconducting materials where, in order to obtain reliable measurements and avoid undesired thermal heating, the use of low DCP is mandatory.[39,40] Clarifying if the $E(J)$ characteristics of manganites are as well affected by a low DCP implies further verification. Thus, to discern between the effects of intrinsic film self-heating ($\sim\rho J^2$) and contact heating ($\sim$DCP$=\rho_c \times I^2$) we have increased $J$ while decreasing $I$ across the films by lithographing narrow stripes, presenting well-defined widths and $\rho_c$, as those shown in the optical micrographs of Figs. 3(a) and 3(b). Simultaneous topographic [Fig. 3(c)] and C-SFM [Fig. 3(d)] images taken on one stripe are also shown to illustrate that the conducting character of the LSMO is preserved in the lithographed region. Figure 2(b) shows a typical set of $E(J)$ curves for a low contact resistivity ($\rho_c < 0.2$ $\mu\Omega$ cm$^2$) sample measured for two temperatures (5 and 300 K) at zero magnetic field, 3 and 5T. Remarkably, now the $E(J)$ characteristics, which overlap each other for a specific temperature, do always present a reproducible linear and nonhysteretic behavior under all conditions. This behavior was found to be preserved in samples with dissipative contact power up to 0.5 W cm$^2$ [Fig. 2(c)]. Moreover, the curves were also found to be independent of the current ramp rate employed, up to 0.1mA/s. We note that, in our experiments the $J$ values reached were pretty high ($J \sim 2\times10^5$ A cm$^{-2}$, depending on the measuring temperature).[25,27,32]

The fact of observing linear $E(J)$ curves without any hysteresis in the LSMO films measured with low DCP values

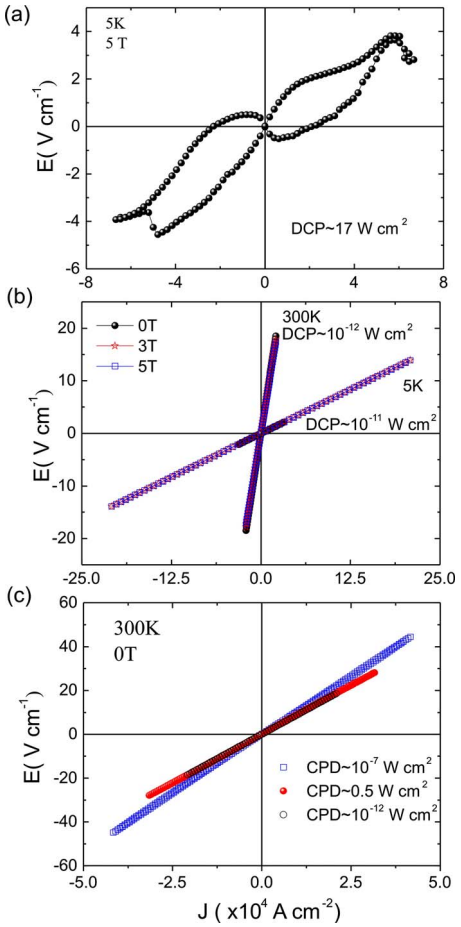


FIG. 2. (Color online) $E(J)$ characteristic curves measured in a four-points configuration for LSMO films with (a) high resistivity contacts (nonlithographed film, DCP $\sim 17$ W cm$^2$); (b) low resistivity contacts at 5 K (DCP $\sim 10^{-11}$ W cm$^2$) and 300K (DCP $\sim 10^{-12}$ W cm$^2$) in a lithographed film. Note that data for different field values overlap at this scale; (c) for different dissipative contact powers in lithographed (DCP $\sim 0.5$ W cm$^2$, ● and DCP $\sim 10^{-12}$ W cm$^2$, ○) and nonlithographed (DCP $\sim 10^{-7}$ W cm$^2$, ■) films. The maximum Joule heating density achieved in these measurements is in the range of $Q \sim 2 \times 10^{12}$ J m$^{-3}$.

allows us to safely conclude that Joule self-heating in LSMO thin films, up to the high $J$ (and $Q$) values used in this paper (Fig. 2) does not induce bistable resistivity. The reason for this can be found through an analysis of the own Joule self-heating and thermal transfer processes. In the adiabatic regime, assuming that Joule self-heating is fully invested in increasing the temperature of the LSMO film, this would be

$$\Delta T = \left[ \int I \times V \mathrm{d}t \right] \Big/ (\mathrm{Vol} \times C_P), \qquad (1)$$

where $I$ is the current through the sample, $V$ the voltage detected, Vol the volume of the sample and $C_P$ the specific heat.[41] This regime results to be a very unrealistic situation because, if it was the case, a rise in temperature of $\Delta T \sim 10^4$ K would be achieved, in complete disagreement with the observed linear $E(J)$ characteristics. The stationary isothermal limit for the thin film, on the other hand, assumes

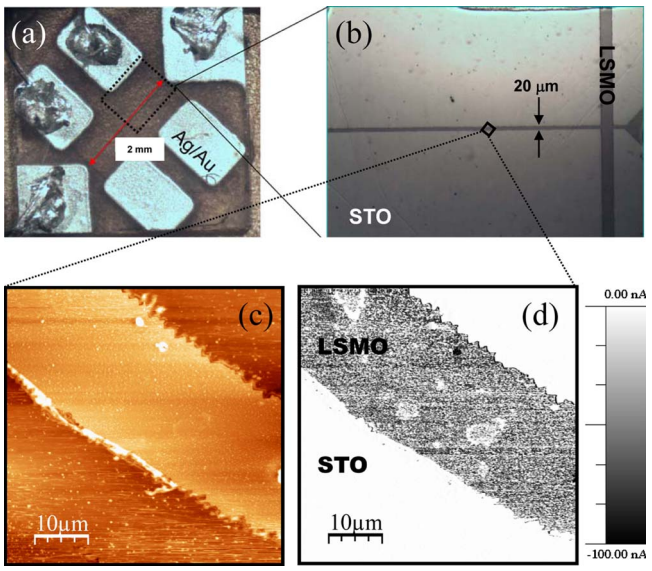


FIG. 3. (Color online) Top: (a) optical micrograph of a lithographed sample and (b) magnification of the lithographed tracks. Bottom: SFM images of (c) topography and (d) local conductivity map at $V_{tip} = -1$ $V$ measured at the lithographed LSMO bridge. The nonconducting character of the bare STO substrate contrasts with the conducting character observed in the LSMO thin film track. The maximum current response corresponds to saturation of the current amplifier, fixed to 100 nA in the experimental set up used.

that the Joule self-heating $Q$ would continuously flow through the substrate toward the thermal bath at which the substrate is thermally anchored. Under this regime no dependence of $E(J)$ on the current ramps should be found, as it is the case in our experiments.

Solving the Fourier equation of thermal transport, including Joule heating of the LSMO film and thermal conduction through the substrate to a thermal bath at fixed temperature $T_B$, the temperature difference between the LSMO film ($T_f$) and the base of the substrate ($T_B$) can be written as

$$\Delta T = T_f - T_B \sim Q t_s t / \kappa_s = \rho(T) J^2 t_s t_f / \kappa_s, \qquad (2)$$

where $t_s$ and $t_f$ are the substrate and film thickness, respectively, and $\kappa_s$ (0.15 W cm$^{-1}$ K$^{-1}$) is the thermal conductivity of the substrate.[42] The consequences of such thermal transport are shown in the upper panels of Fig. 4. The result of estimating $\Delta T$ along the $E(J)$ curves is depicted as a color scale.

We first asses the case of maximum $Q = \rho J^2 = EJ$ values ($J \sim 5 \times 10^4$ A cm$^{-2}$, $Q \sim 2 \times 10^{12}$ J m$^{-3}$) resulting from data at $T_B = 300$ K in Fig. 2(c), and which are higher or similar than most of the commonly used values. The calculated $T_f$ values differ from $T_B$ at most by about 1.5 K. This temperature increase [represented by the color scale in Fig. 4(a)], induces relative resistivity changes $\Delta\rho(T)/\rho(T) \sim 2\%$, within the LSMO film and hence linear $E(J)$ curves are measured within this Joule self-heating regime. Now we compare with what happened when the transport measurements at 300 K were carried out up to higher $J$ values ($J \sim 1 \times 10^5$ A cm$^{-2}$) LSMO thin film and a DCP $\sim 10^{-7}$ W cm$^2$. Figure 4(b) displays a typical $E(J)$ curve where a volume

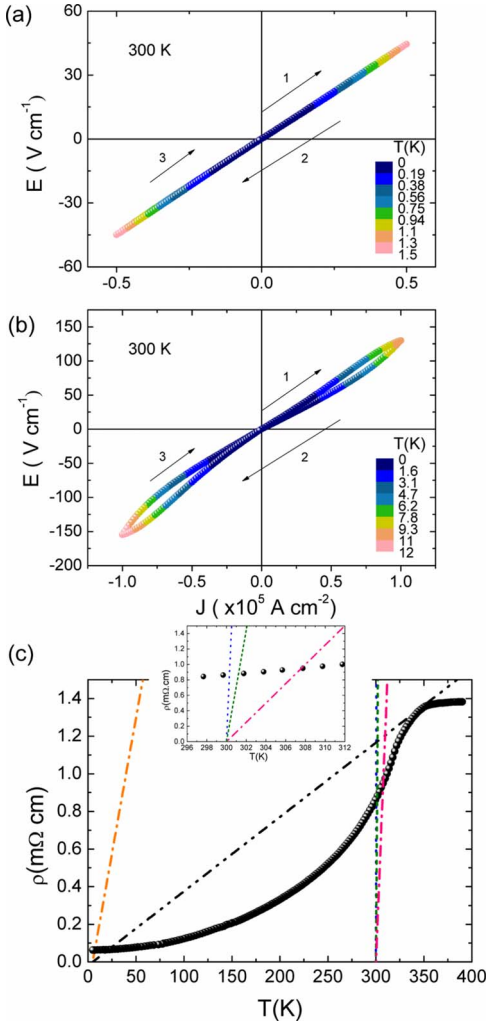


FIG. 4. (Color online) $E(J)$ curves measured at 300 K and zero magnetic field in nonlithographed LSMO thin films up to $J_{max}=5\times10^4$ A cm$^{-2}$ (a) and $J_{max}=10^5$ A cm$^{-2}$ (b). The calculated temperature increases based on a steady heat transfer through the substrate is indicated by a color code as indicated. (c) Main panel: Representation of the two members of Eq. (3), i.e., the resistivity under zero magnetic field data of Fig. 1 (●) and $\kappa_s/J^2\, t_s t_f$ $(T-T_B)$ for lithographed and nonlithographed films. For $T_B=300$ K, the three straight lines with decreasing slope, each for the experimental values $J=2\times10^4$ A cm$^{-2}$, $J=5\times10^4$ A cm$^{-2}$, and $J=1\times10^5$ A cm$^{-2}$, respectively, were used to obtain the corresponding $T_f$. The steeper line corresponds to the lithographed film. The inset is a magnification of the 300 K region to show the small rise in temperature. For comparison, two extreme cases are shown, in the main panel, for $T_B=5$ K: the maximum $J$ value employed in the presented experiments ($J=2\times10^5$ A cm$^{-2}$, large slope line) and a typical $J$ value ($J=5\times10^5$ A cm$^{-2}$, low slope line) required to have bistability (see text).

dissipation $Q\sim10^{13}$ J m$^{-3}$ could be reached. It is clearly seen that some nonlinearity and $E(J)$ hysteresis is induced under these conditions without any transition to a second stable resistance (resistance bistability). Within the scenario described above, i.e., a steady isothermal state for LSMO film with Joule heat flowing through the substrate, the film temperature would increase [Eq. (2)] by $\Delta T\sim11-12$ K (see color scale in the figure). This temperature increase induces relative resistivity changes $\Delta\rho(T)/\rho(T)\sim8\%$ within the LSMO film. The observed resistivity increase in Fig. 4(b) is consistent with the experimental $\rho(T)$ curve in Fig. 1, therefore validating the use of this thermal transfer model.

To visualize the stable temperatures which might exist in a LSMO film measured at $J$ and having a firm thermal anchoring, we rewrite Eq. (2) in the following way:

$$\rho(T_f)=(\kappa_s/J^2 t_s t_f)(T_f-T_B). \tag{3}$$

For each $J$, the stable film temperatures ($T_f$), accordingly to thermal transfer model, can be found by looking for the intersection points of the experimental $\rho(T)$ and the straight lines starting at $T_B$ and with slopes $\kappa_s/J^2 t_s t_f$. In order to show that, the resistivity under zero magnetic field shown in Fig. 1 is displayed now in Fig. 4(c) together with the straight lines corresponding to a series of representative $J$ values used in the $E(J)$ experiments ($T_B=300$ K) for lithographed and nonlithographed samples (details are given in the figure caption). The inset shows a magnification of the 300K region where it is easy to verify the final temperature for the extreme $J$ values. The crossing points with $\rho(T)$ determine the corresponding resistivity, $\rho(T_f)$, and film temperature ($T_f$) values, which are fully consistent with those determined in the $E(J)$ curves reported in the top and medium panels of the figure.

From the shape of the $\rho(T)$ curve and the corresponding $\kappa_s/J^2 t_s t_f$ lines, it is clearly seen that the straight lines starting at $T_B$ could have two intersection points with $\rho(T)$ when $T_B$ is below $\sim250$ K. Hence, bistable resistivity of thermal origin in LSMO films having a firm thermal anchoring can only be achieved below this temperature. For instance, measurements performed at $T_B=5$ K in lithographed films would require measuring with $J>5.2\times10^5$ A/cm$^2$ to detect resistance bistability, i.e., intrinsic self-heating bistable resistivity would only occur in LSMO thin films at very high current densities. Our results point therefore to the fact that either contact heating or low thermal anchoring of the films may have strongly influenced previous measurements showing resistance bistability at high temperatures in LSMO thin films.

Aimed by the nowadays increasing interest of applying the bistability performances at miniaturization levels,[2,43,44] we have also addressed the influence of the electric contacts quality at the nanometer scale. In order to that, we have performed C-SFM measurements on the same LSMO films onto which Au nanoparticles were dispersed as described above. Figure 5(a) shows the current map taken at 0.5V where the Au nanodots are clearly visualized as highly conducting dots. Instead of the macroscopic $E(J)$ characteristics curves, now current versus voltage ($I$-$V$) curves [Fig. 5(b)] were obtained as detailed in the experimental section. When the tip was brought into direct contact with the LSMO films, i.e., at the bare regions between nanodots, the $I$-$V$ curves fairly well-reproduced the nonlinear behavior generally observed so far in this type of measurements. Occasionally, these curves displayed some irreproducible hysteretic shape, questioning the quality of the contact. To ensure a good electrical junction (nature and contact area) at the nanoscale during the $I$-$V$ measurements, the conductive tip was then placed on top of Au nanodots. Figure 5(c) displays a typical

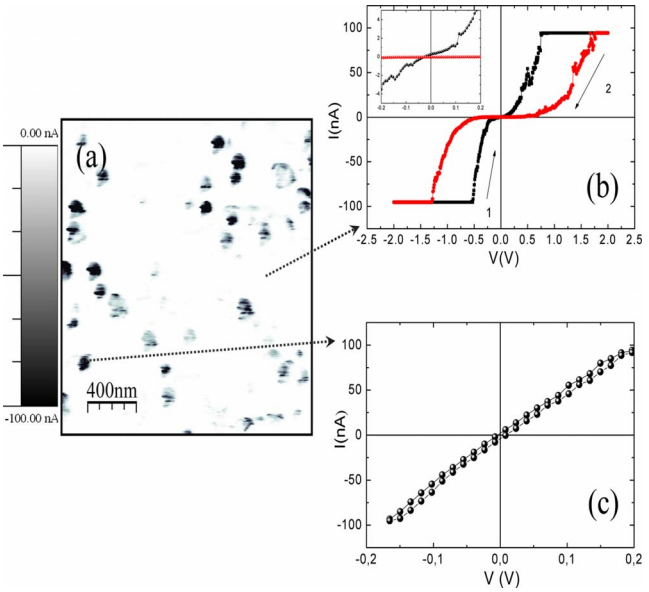


FIG. 5. (Color online) (a) Current SFM image (5 $\mu$m $\times 5$ $\mu$m) of a LSMO film surface where Au dots have been deposited (see text for details). The Au dots are easily identified at a small sensing bias. (b) Typical *I-V* curve measured under direct contact between tip and LSMO surface. (c) Typical *I-V* curve measured through a contact of the tip on top of the Au nanodots. Flat regions response in the current are due to the saturation of the current amplifier, fixed to 100 nA in the experimental set up used.

*I-V* curve in this case. The curves were found to be very reproducible and present a linear and reversible behavior, indicating ohmic contacts between the Au dots and the metallic LSMO films, as well as between the C-SFM tip and the Au nanodots. We remark that this linear behavior exists even beyond much larger *I* values than those measured for the direct contact. If we now analyze the involved magnitudes, in particular the contact resistances derived from the inverse slope at low voltages, we note that for similar *J* values, the estimated DCP ratio between tip-sample and tip-Au nanodot-sample contact lie in the range DCP(tip-LSMO)/DCP(tip-Au-LSMO) $\sim 10^3 - 10^5$. To estimate DCP, the nanodot diameter was used to calculate the contact area in the tip-Au-film case, whereas for direct tip-film contact it was calculated using the Hertzian model.[45]

In summary, as in macroscopic measurements, linear and reversible *I-V* curves are recorded at nanometer junctions when using configurations with a low electrical contact resistance, while nonlinear and hysteretic curves are obtained when poor electrical contacts (direct tip-film contact) are used. This is observed even at low voltages as seen in the inset in Fig. 5(b). In the latter case, additionally, the reproducibility of the curves is deficient because of the variability of the electrical resistance on repeated contacts. This nanoscale experiment further confirms that undesired Joule heating induced by contact heating may control *I-V* measurements in LSMO films unless proper care of the experimental set up is considered. Our finding supports the macroscopic measurements showing that an intrinsic Joule self-heating bistable behavior does not exist in the LSMO films at 300 K.

In this paper, we have shown that macroscopic transport and nanoscale current versus voltage measurements in $La_{0.7}Sr_{0.3}MnO_3$ thin films remain linear and nonhysteretic up to very stringent self-heating regimes when low dissipative contact powers are achieved. We have particularly shown that when $E(J)$ measurements are performed at 300 K up to $J \sim 5 \times 10^4$ A cm$^{-2}$ (Joule self-heating $Q = \rho J^2 = 2 \times 10^{12}$ J m$^{-3}$) only a moderate rise in temperature ($\Delta T < 1.5$ K) is calculated in the scope of a stationary thermal transfer model for the thin film, the $E(J)$ curves remaining linear. A noticeable hysteresis in the $E(J)$ curve is detected instead when the current density is increased up to $J \sim 10^5$ A/cm$^2$ ($Q = 10^{13}$ J m$^{-3}$) which corresponds to $\Delta T \sim 12$ K.

We have further demonstrated that, under adequate measuring conditions, a regime of bistable resistivity in LSMO thin films is not achieved at $T = 300$ K. We otherwise suggest that this phenomenon would only occur in LSMO films when measuring at temperatures below $T \sim 250$ K. The best geometry to achieve this regime being a lithographed film where very high current densities could be achieved without detrimental effects associated to the electrical contacts which would perturb the thermal profile of the film. Nonlinearity and hysteretic behavior have been indeed observed both in macroscopic and in nanoscale measurements, when the dissipative contact power is high. Obviously, our conclusion do not question the existence of bistable resistivity in other oxides, including several manganite phases previously investigated, such as $Pr_{1-x}Ca_xMnO_3$ or $Nd_{1-x}Ca_xMnO_3$,[4,23,46,47] or in devices based on LSMO where some role of the metallic interfaces has been identified but still not completely clarified. It neither invalidates any proposal concerning the microscopic origin of this phenomenon. Our experiments strongly suggest, however, that in order to firmly conclude about the origin of the intrinsic mechanisms operating in resistance switching, the influence of contact heating and Joule self-heating need to be properly weighted.

Our analysis stresses the very relevant role played by thermal heating generated at the electrical contacts in the investigation of high current transport measurements. As what it concerns the origin of the electroresistance phenomenon in oxides (i.e., bistable resistance) it is still a controversial matter involving the influence of the nature of the interfacial contacts with metals and therefore it falls outside the scope of this paper.

We acknowledge the financial support from MEC (Grants. No. CONSOLIDER CSD2007-00041 NANOSELECT, No. MAT2005-02047, No. NAN2004-09133-C03-01, No. MAT2006-26543-E, No. MAT2007-62732, and No. MAT2008.01022/NAN), Generalitat de Catalunya (Grants No. Pla de Recerca SGR-0029 and No. CeRMAE), CSIC (Grant No. PIF-CANNAMUS) and EU (Grants No. HIP-ERCHEM, and No. NESPA). J.G. would like to thank MEC-FPU program.

*cmoreno@icmab.es

[1] G. I. Meijer, Science **319**, 1625 (2008).
[2] K. Szot, W. Speier, G. Bihlmayer, and R. Waser, Nature Mater. **5**, 312 (2006).
[3] Y. B. Nian, J. Strozier, N. J. Wu, X. Chen, and A. Ignatiev, Phys. Rev. Lett. **98**, 146403 (2007).
[4] M. J. Rozenberg, I. H. Inoue, and M. J. Sanchez, Phys. Rev. Lett. **92**, 178302 (2004).
[5] D. B. Strukov, G. S. Snider, D. R. Stewart, and R. S. Williams, Nature (London) **453**, 80 (2008).
[6] J. J. Yang, M. D. Pickett, X. M. Li, D. A. A. Ohlberg, D. R. Stewart, and R. S. Williams, Nat. Nanotechnol. **3**, 429 (2008).
[7] R. Waser and M. Aono, Nature Mater. **6**, 833 (2007).
[8] A. Beck, J. G. Bednorz, C. Gerber, C. Rossel, and D. Widmer, Appl. Phys. Lett. **77**, 139 (2000).
[9] M. Janousch, G. I. Meijer, U. Staub, B. Delley, S. F. Karg, and B. P. Andreasson, Adv. Mater. **19**, 2232 (2007).
[10] A. Chen *et al.*, IEEE Int. Electron Devices Meet., Tech. Dig. **1089**, 765 (2005).
[11] S. H. Chang, J. S. Lee, S. C. Chae, S. B. Lee, C. Liu, B. Kahng, D. W. Kim, and T. W. Noh, Phys. Rev. Lett. **102**, 026801 (2009).
[12] B. J. Choi *et al.*, J. Appl. Phys. **98**, 033715 (2005).
[13] M. Chang, Y. Ju, J. Lee, S. Jung, H. Choi, M. Jo, S. Jeon, and H. Hwang, Appl. Phys. Lett. **93**, 022101 (2008).
[14] A. Baikalov, Y. Q. Wang, B. Shen, B. Lorenz, S. Tsui, Y. Y. Sun, Y. Y. Xue, and C. W. Chu, Appl. Phys. Lett. **83**, 957 (2003).
[15] F. A. Chudnovskii, L. L. Odynets, A. L. Pergament, and G. B. Stefanovich, J. Solid State Chem. **122**, 95 (1996).
[16] S. Q. Liu, N. J. Wu, and A. Ignatiev, Appl. Phys. Lett. **76**, 2749 (2000).
[17] C. Rossel, G. I. Meijer, D. Bremaud, and D. Widmer, J. Appl. Phys. **90**, 2892 (2001).
[18] I. H. Inoue and M. J. Rozenberg, Adv. Funct. Mater. **18**, 2289 (2008).
[19] S. Tsui, A. Baikalov, J. Cmaidalka, Y. Y. Sun, Y. Q. Wang, Y. Y. Yue, C. W. Chu, L. Chen, and A. J. Jacobson, Appl. Phys. Lett. **85**, 317 (2004).
[20] A. Odagawa, T. Kanno, and H. Adachi, J. Appl. Phys. **99**, 016101 (2006).
[21] A. V. Gurevich and R. G. Mints, Rev. Mod. Phys. **59**, 941 (1987).
[22] S. Balevicius, N. Zurauskiene, V. Stankevic, P. Cimmperman, S. Kersulis, A. Cesnys, S. Tolvaisiene, and L. L. Altgilbers, Appl. Phys. Lett. **90**, 212503 (2007).
[23] A. S. Carneiro, R. F. Jardim, and F. C. Fonseca, Phys. Rev. B **73**, 012410 (2006).
[24] Y. F. Chen and M. Ziese, J. Appl. Phys. **101**, 103902 (2007).
[25] Y. F. Chen, M. Ziese, and P. Esquinazi, Appl. Phys. Lett. **88**, 222513 (2006).
[26] S. Mercone, R. Fresard, V. Caignaert, C. Martin, D. Saurel, C. Simon, G. Andre, P. Monod, and F. Fauth, J. Appl. Phys. **98**, 023911 (2005).
[27] A. Palanisami, M. B. Weissman, and N. D. Mathur, Phys. Rev. B **71**, 094419 (2005).
[28] J. Sacanell, A. G. Leyva, and P. Levy, J. Appl. Phys. **98**, 113708 (2005).
[29] H. Song, M. Tokunaga, S. Imamori, Y. Tokunaga, and T. Tamegai, Phys. Rev. B **74**, 052404 (2006).
[30] J. C. Wu, H. Sun, H. X. Da, and Z. Y. Li, Appl. Phys. Lett. **91**, 102501 (2007).
[31] A. Asamitsu, Y. Tomioka, H. Kuwahara, and Y. Tokura, Nature (London) **388**, 50 (1997).
[32] S. Imamori, M. Tokunaga, S. Hakuta, and T. Tamegai, Appl. Phys. Lett. **89**, 172508 (2006).
[33] H. K. Lau and C. W. Leung, J. Appl. Phys. **104**, 123705 (2008).
[34] Y. W. Xie, J. R. Sun, D. J. Wang, S. Liang, and B. G. Shen, J. Appl. Phys. **100**, 033704 (2006).
[35] A. Hassini, A. Pomar, J. Gutierrez, M. Coll, N. Roma, C. Moreno, A. Ruyter, T. Puig, and X. Obradors, Supercond. Sci. Technol. **20**, S230 (2007).
[36] C. Moreno *et al.*, Adv. Funct. Mater. **19**, 2139 (2009).
[37] I. Horcas, R. Fernandez, J. M. Gomez-Rodriguez, J. Colchero, J. Gomez-Herrero, and A. M. Baro, Rev. Sci. Instrum. **78**, 013705 (2007).
[38] A stable aqueous colloidal solution (105 mg/l) of citrate-stabilized gold nanoparticles was obtained by using trisodium citrate for the reduction in chloroauric acid ($HAuCl_4$) and provided by Dauchot-Weymeers (Université Libre de Bruxelles).
[39] J. W. Ekin, C. C. Clickner, S. E. Russek, and S. C. Sanders, IEEE Trans. Appl. Supercond. **5**, 2400 (1995).
[40] J. Gutiérrez *et al.*, Nature Mater. **6**, 367 (2007).
[41] J. L. Cohn, J. J. Neumeier, C. P. Popoviciu, K. J. McClellan, and T. Leventouri, Phys. Rev. B **56**, R8495 (1997).
[42] E. F. Steigmeier, Phys. Rev. **168**, 523 (1968).
[43] X. Chen, N. J. Wu, J. Strozier, and A. Ignatiev, Appl. Phys. Lett. **89**, 063507 (2006).
[44] C. Yoshida, K. Kinoshita, T. Yamasaki, and Y. Sugiyama, Appl. Phys. Lett. **93**, 042106 (2008).
[45] A typical $F=50$ nN is considered. A tip radius of 25 nm was estimated from line profiles across the Au nanodots, whose diameters were 10–15 nm as evidenced by TEM and IR absorption. For our tip-LSMO system, the respective Young moduli ($E$) and Poisson ratios ($\nu$) are: $E_{tip}=1000$ GPa and $\nu_{tip}=0.15$, and $E_{LSMO}=500$ GPa (Ref. 48) and $\nu_{LSMO}=0.38$ (obtained from XRD and TEM measurements).
[46] M. Quintero, P. Levy, A. G. Leyva, and M. J. Rozenberg, Phys. Rev. Lett. **98**, 116601 (2007).
[47] A. Sawa, T. Fujii, M. Kawasaki, and Y. Tokura, Appl. Phys. Lett. **88**, 232112 (2006).
[48] K. Steenbeck, T. Habisreuther, C. Dubourdieu, and J. P. Senateur, Appl. Phys. Lett. **80**, 3361 (2002).